Two-channel spectroscopic reflectometry for *in situ* monitoring of blanket and patterned structures during reactive ion etching

Brooke S. Stutzman
Applied Physics Program, University of Michigan, Ann Arbor, Michigan 48109

Hsu-Ting Huang
Department of Electrical Engineering and Computer Science, University of Michigan, Ann Arbor, Michigan 48109

Fred L. Terry, Jr.[a)]
Applied Physics Program and Department of Electrical Engineering and Computer Science, University of Michigan, Ann Arbor, Michigan 48109

(Received 21 January 2000; accepted 2 October 2000)

In this article we present a low-cost, high-speed, high-accuracy *in situ* thin film measurement system for real-time process monitoring and industrial process control. This sensor, the two-channel spectroscopic reflectometer (2CSR), is a hybrid of spectroscopic ellipsometry and spectroscopic reflectometry. In 2CSR a polarized beam of white light is directed at the sample. The reflected light is resolved into its two orthogonal components, *s* and *p*, using a Wollaston prism. These data, $|R_s|^2$ and $|R_p|^2$, are recorded simultaneously as a function of wavelength using a two-channel spectrometer with linear array detectors. The fact that 2CSR has no moving parts, coupled with the use of the two-channel linear array detectors, enables high-accuracy data acquisition across the sensor's spectral range in 6 ms. This makes the 2CSR ideal for real-time high-speed process monitoring and control in an industrial setting. We have used the 2CSR to make accurate *in situ*, high speed film thickness measurements during the plasma etching of both silicon dioxide and polycrystalline silicon samples. We show that, in addition to our ability to measure blanket film thicknesses and etch rates, the accuracy of the 2CSR makes this a viable technique for patterned wafer analysis. © *2000 American Vacuum Society.* [S0734-211X(00)19006-7]

I. INTRODUCTION

Plasma processes are critical in device fabrication. Many of these processes continue to be timed etches and depositions. However, as film thicknesses and linewidths are reduced to nanometer scales, process control is needed in order to ensure device quality. Before process control can be implemented, however, sensors capable of providing useful information in real time are necessary.[1–5] These sensors must also be robust to vibration and other such factors found in industrial manufacturing settings. Additionally, they must be affordable so as to make it cost effective to implement process control on a wide-scale basis.

Optical sensors are ideal for *in situ* metrology in plasma-based systems.[6] Two such sensors for monitoring the wafer state during plasma processing are spectroscopic ellipsometry (SE)[7–13] and normal incidence spectroscopic reflectometry (SR).[1,14,15] Both of these measurement systems are based on thin film interference. In SR, the intensity of the reflected light beam is measured as a function of wavelength. These intensity data are then converted to absolute reflectances as a function of wavelength by normalizing with respect to a known calibration standard. These reflectance data vary in an approximately periodic manner with the film thickness due to the interference effects. In some cases where the reflectance data have sufficiently unique structure, parametric models for the optical dielectric function of the thin film can be fitted as well as the thickness.

Previous work in our group demonstrated SR film thickness measurements on millisecond time scales.[1] This high-speed data acquisition capability and the facts that SR has no moving parts and is inexpensive make SR a potential candidate for industrial process monitoring and control. However, the major disadvantages of SR are the dependence on a calibration standard, the stability of the intensity measurement, and a comparatively low sensitivity to very thin films.

SE is a fundamentally more accurate technique than SR for obtaining film thickness and optical dielectric function information. In general, SE measurements are performed at an angle off-normal with respect to the sample. In this configuration, the measurement is sensitive to the state of polarization of the incident and reflected waves.[16] The measured data are generally written in the form of the ratio, ρ, of the complex Fresnel reflection coefficients for the *s* and *p* polarizations, r_s and r_p, respectively,

$$\rho = r_p / r_s \tag{1}$$

or

$$\rho = \tan(\psi) e^{i\Delta}, \tag{2}$$

where $\tan(\psi)$ is the ratio of the magnitude of the *p*-polarized to the *s*-polarized reflected light ($|r_p|/|r_s|$) and Δ is $\delta_{r_p} - \delta_{r_s}$. δ_{r_p} and δ_{r_s} indicate the phase shifts upon reflection for the *p* and *s* polarizations, respectively. SE can be applied *in*

[a)]Electronic mail: fredty@umich.edu

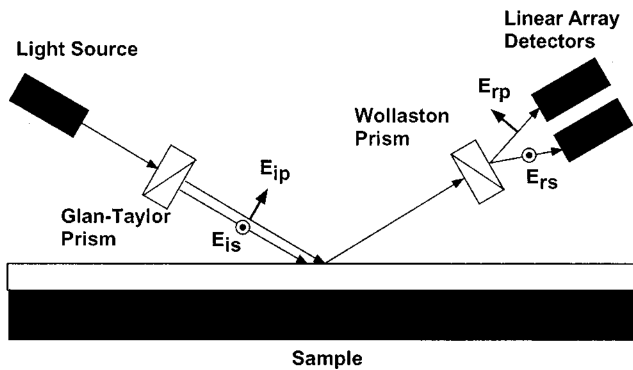

FIG. 1. Schematic of 2CSR setup. The Glan–Taylor prism fixes the polarization of the incident light. The Wollaston prism resolves the light reflected from the sample into its *s* and *p* components. The spectral intensities of the two exit beams from the Wollaston prism are then recorded simultaneously by a spectrometer with two linear array detectors.

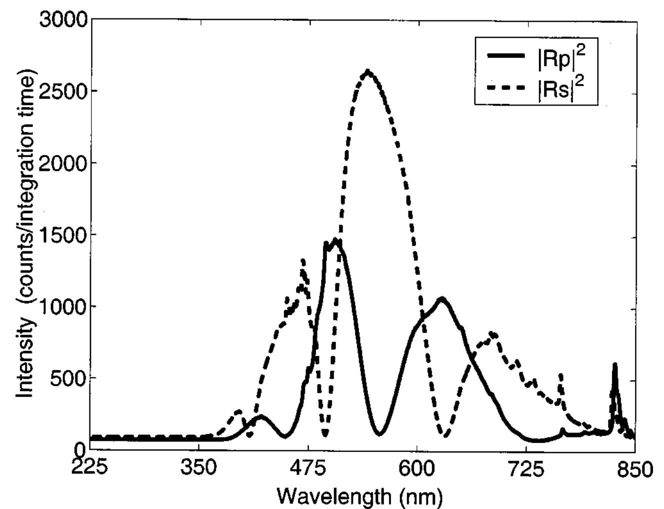

FIG. 2. Raw data from 2CSR measurement of 1 μm silicon dioxide on silicon. $|R_p|^2$ is shown by a solid line and $|R_s|^2$ is shown by a dashed line.

situ[17–24] and is robust to shop floor conditions. Additionally, data acquisition times in the tens of milliseconds have been reported.[25–28] However, in general, in order to obtain good signal-to-noise ratios on these time scales, more expensive detectors must be used. Also, the moving components make commercial SEs more susceptible to mechanical failure.

Single wavelength and spectroscopic reflectometry can be done in off-normal configurations as well. However, in these cases, the polarization dependent reflection coefficients must be considered as in the ellipsometry case.[29–31]

In this article, we present what we believe to be the first such spectroscopic sensor which simultaneously measures both the *p*- and the *s*-polarized reflected intensities ($|R_p|^2$ and $|R_s|^2$) over a broad spectral range (see Fig. 1). This sensor, the two-channel spectroscopic reflectometer (2CSR) combines the simplicity and lack of moving parts characteristic of SR with the use of an analyzer (in this case a Wollaston prism) as in SE and a low-cost, two-channel spectrometer, in order to obtain near-ellipsometric accuracy measurements in as little as 6 ms. This makes 2CSR ideal for process monitoring of transient phenomena and industrial process control. Additionally, the level of accuracy of the 2CSR measurements allows us to apply the technique to patterned wafer analysis.

II. 2CSR SYSTEM

The 2CSR system configuration is illustrated in Fig. 1. The key elements of the system are the simultaneous resolution of the broad-spectrum light into *s* and *p* polarizations using a Wollaston prism and the spectral analysis of these two orthogonal components using low-cost linear array spectrometers. The use of the Wollaston prism in such measurements dates back to the beginning of the 20th century,[32–35] however, it was not until the work of Jellison and Modine in 1990 that the prism was used for spectroscopic thin film measurements.[36] The recent availability of low-cost charge coupled device (CCD) spectrometers allows us to use multiple spectrometers on a single system. By using two spectrometers, we are able to simultaneously record the two orthogonally polarized exit beams from the Wollaston prism over a broad wavelength range on millisecond timescales.

We use a 75 W xenon arc lamp as our light source. Our polarizer is an ultraviolet (UV) grade calcite Glan–Taylor prism with an extinction ratio of 5×10^{-5} and a beam deviation of 1 min of arc. We fix polarization of the incident beam at 45° for these experiments. In order to avoid any stress-induced polarization changes we use strain-free windows on the ellipsometer ports of the reactive ion etch (RIE) chamber which we used as a testbed for this sensor. Our RIE chamber is a parallel plate, capacitively coupled reactor which is a scaled-up version of the Gaseous Electronics Conference (GEC) reference cell.[37] We place the sample on the bottom electrode (the powered electrode) of the modified GEC cell. The spot size of the light hitting the sample is approximately 1 cm by 3 cm. The extinction ratio of the calcite Wollaston prism is 10^{-6} and the angle between the exiting beams is nominally 20° for 546 nm light and varies by approximately 5° within our wavelength range. We use UV grade collimating beam probes to refocus the two exit beams from the Wollaston prism into fiber optic cables.

We collect these intensity data using an Ocean Optics SD2000 two-channel spectrometer. Each spectrometer uses a fixed position, 600 lines/mm grating blazed for 400 nm, a 25 μm entrance slit, and a 2048 element linear CCD array with a selective coating to reduce second order effects. The spectral resolution is 1.3 nm. We collect both *s*- and *p*-polarized data simultaneously over the range 370–850 nm in 6 ms. An example of the raw data is shown in Fig. 2. Acquisition speed can be improved (with reduced signal to noise) to 3 ms with currently available analog-to-digital cards. We believe that the UV performance of the 2CSR is primarily limited by the Wollaston prism and the near infrared performance is limited by the CCD detectors and the xenon lamp intensity.

We determined our incident angle to be $73.00°\pm0.05°$ by measuring $|R_s|^2$ and $|R_p|^2$ for a well known silicon dioxide/silicon sample and doing a least squares fit of the incident angle.[18] In SE one would determine the incident angle by

making a measurement of a bare silicon sample and doing a two parameter least squares fit of the incident angle and the oxide overlayer thickness. We are operating the 2CSR near the pseudo-Brewster angle of silicon (76.13° at 546.1 nm)[16] so the p-reflected intensity is minimal. In ellipsometry, this means that the $\tan(\psi)$ value is close to zero, however, the phase information found in $\cos(\Delta)$ has enough structure that meaningful information about the sample and the angle of incidence can be derived from this parameter alone. Since 2CSR measures the absolute reflected intensity of the s- and p-reflected light, with a bare silicon substrate we ostensibly can only fit the s-intensity data to an optical model. However, the s-reflected intensity from a bare silicon wafer does not have sufficient structure for us to definitively determine the angle of incidence. By using a well-known thick oxide rather than a bare silicon wafer for this angle of incidence calibration, we obtain strong s- and p-reflected intensity data from the sample. These data have enough structure that we can fit to the optical model in order to determine the incident angle. This calibration need only be performed when the sensor is first placed on a piece of equipment.

In order to account for run-to-run variations in the system, such as fluctuations in intensity of the light source and in the wavelength dependent sensitivity of the detectors, an absolute intensity calibration must be performed. All experimental data must be normalized with respect to this calibration. The frequency with which this calibration needs to be repeated depends on the overall stability of the light source and the detector. Although our current system will typically yield accurate results several hours after initial calibrations, we repeat this calibration for each measurement to account for the fluctuations in the intensity of the light source and the gain changes in the detectors due to temperature variations. By adding feedback stabilization of the lamp intensity and the detector temperature, accurate operation with long periods between calibrations should be possible.

The calibration procedure requires two steps. First, a reference spectrum is collected from mirror smooth, magnetron sputtered aluminum on silicon sample. We chose aluminum as a reference rather than bare silicon because aluminum has a high reflectance for both the s and p polarizations of light. When exposed to air, the aluminum grows an oxide overlayer 20–25 Å thick, as does bare silicon. In general, this overlayer cannot be neglected when making optical measurements. For instance, the in ellipsometric measurements, the native oxide on aluminum can cause a 18% decrease in the calculated refractive index, n, at 546 nm and the extinction coefficient, k, is low by 10% at the same wavelength.[38] However, we are not making a phase-sensitive ellipsometric measurement; we are looking at the absolute reflected intensities of the s and p polarizations. As mentioned in the previous paragraph, when the p-reflected intensity is close to zero, as it is near the pseudo-Brewster condition, the ellipsometric parameter $\tan(\psi)$ is close to zero as well and SE fits in this regime rely on fitting the phase information found in $\cos(\Delta)$. Thus, a small change in surface layer thickness due to the growth of a native oxide, if neglected, will cause a significant change in the determined film properties. In order to assess what effect, if any, the native oxide has on our calibration, we modeled the orthogonally polarized 73° reflected intensities from both a bare aluminum sample and an aluminum sample covered with a 20 Å oxide overlayer. In Fig. 3, we plot $(|R_{s_{\text{bare}}}|^2/|R_{s_{\text{oxide}}}|^2)_{\text{Al}}$ and $(|R_{p_{\text{bare}}}|^2/|R_{p_{\text{oxide}}}|^2)_{\text{Al}}$ over the wavelengths used in our measurements. $(|R_{s_{\text{bare}}}|^2/|R_{s_{\text{oxide}}}|^2)_{\text{Al}}$ ranges from 1.001 to 1.000 and $(|R_{p_{\text{bare}}}|^2/|R_{p_{\text{oxide}}}|^2)_{\text{Al}}$ ranges from 0.992 to 0.995. Thus, at most, the aluminum oxide overlayer causes a 0.1% change in the $|R_s|^2_{\text{Al}}$ data and a 0.8% change in the $|R_p|^2_{\text{Al}}$ data. In comparison, Fig. 4 shows $(|R_{s_{\text{bare}}}|^2/|R_{s_{\text{oxide}}}|^2)_{\text{Si}}$ and $(|R_{p_{\text{bare}}}|^2/|R_{p_{\text{oxide}}}|^2)_{\text{Si}}$ for bare silicon and silicon with a native oxide over the same wavelengths. $(|R_{s_{\text{bare}}}|^2/|R_{s_{\text{oxide}}}|^2)_{\text{Si}}$ ranges from 1.01 to approximately 1.00 and $(|R_{p_{\text{bare}}}|^2/|R_{p_{\text{oxide}}}|^2)_{\text{Si}}$ ranges from 0.95 to 0.97. From this, we see that the maximum error caused by an oxide overlayer on silicon substrate is an order of magnitude greater error (1% vs 0.1%) than that of an oxide overlayer on an aluminum substrate. Furthermore, the error in the $|R_p|^2_{\text{Si}}$ data caused by an oxide overlayer ranges from 3%–5% compared to a maximum error of less than 1% for the aluminum sample.

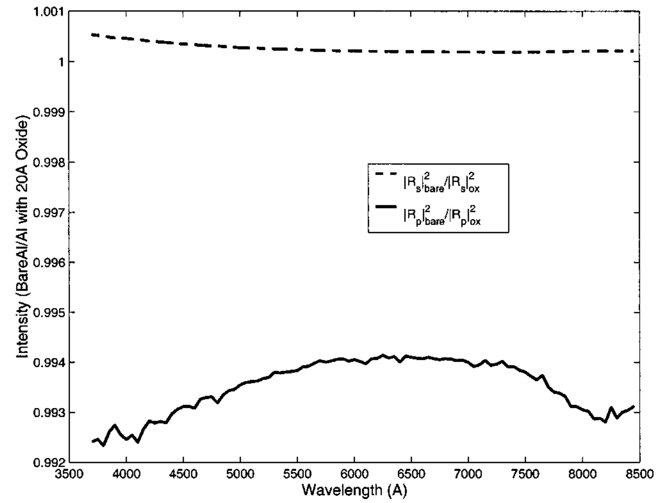

FIG. 3. Error incurred by neglecting oxide overlayer in 73° measurement of $|R_s|^2$ and $|R_p|^2$ from an aluminum sample. The ratio of the calculated s-reflected intensity from a bare aluminum sample to the calculated s-reflected intensity from an aluminum sample with an oxide surface layer is shown by the dashed line. The ratio of the calculated p-reflected intensity from a bare aluminum sample to the calculated p-reflected intensity from an aluminum sample with an oxide surface layer is shown by the solid line.

The difference in the effect of an oxide overlayer on an aluminum sample versus the effect of an oxide overlayer on a bare silicon sample is due to the fact that for absorbing material, such as a semiconductor or metal, the p-polarized reflectance does not go to zero for any angle of incidence. Instead, there is a pseudo-Brewster condition at which the reflected p intensity is at a minimum. This condition occurs at an incident angle which depends on the extinction coefficient, k.[16] The Brewster condition is shown in the following equation:

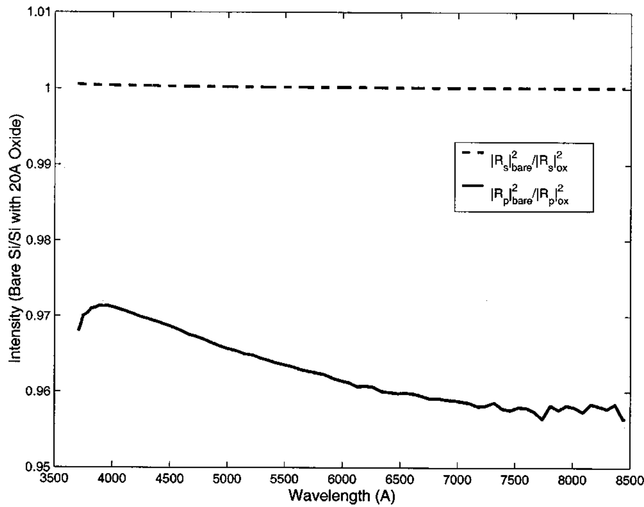

FIG. 4. Error incurred by neglecting oxide overlayer in 73° measurement of $|R_s|^2$ and $|R_p|^2$ from a silicon sample. The ratio of the calculated *s*-reflected intensity from a bare silicon sample to the calculated *s*-reflected intensity from a silicon sample with an oxide surface layer is shown by the dashed line. The ratio of the calculated *p*-reflected intensity from a bare silicon sample to the calculated *p*-reflected intensity from a silicon sample with an oxide surface layer is shown by the solid line.

$$\tan(\phi_B) = \frac{N_1}{N_0}, \tag{3}$$

where ϕ_B is the Brewster angle and N_0 and N_1 are the complex indices of refraction of the ambient and substrate, respectively. Since k ranges from approximately 0.01 to 1.0 over our wavelength range for silicon, Equation (3) is quasireal and the *p*-reflected intensity is approximately zero at the pseudo-Brewster condition. The value of k for aluminum, however, ranges from roughly 4 to 9 over our wavelength range. Thus, for aluminum, Eq. (3) is never quasireal. Consequently, aluminum has a high reflectivity for both the *s* and *p* polarizations of light. Due to this high reflectivity, the bulk material properties of aluminum dominate the reflectance measurements and thin oxide overlayer effects do not significantly change the reflected intensities of either the *s*- or *p*-polarized light. Conversely, for silicon, the *p*-reflected intensity is close to zero at the pseudo-Brewster condition, so the addition of any oxide overlayer will have a greater effect on the *p*-polarized reflected intensity. This will lead to the deviation from the bare silicon model we see in Fig. 4.

After taking the reference spectra from the aluminum sample, we continue the calibration procedure by taking a measurement with the light source blocked in order to determine the background counts. We then place the sample to be measured in the chamber and data are collected. These data are normalized using the following equation:

$$I_{s(p)}(\lambda) = \frac{[I_{s(p)\text{meas}}(\lambda) - I_{s(p)\text{bkg}}(\lambda)]}{[I_{s(p)\text{ref}}(\lambda) - I_{s(p)\text{bkg}}(\lambda)]} I_{s(p)\text{th,ref}}(\lambda), \tag{4}$$

where $I_{s(p)}$ is the wavelength dependent normalized reflected intensity of the $s(p)$ polarized light, $I_{s(p)\text{meas}}$ is the measured reflected intensity from the sample, $I_{s(p)\text{bkg}}$ is the measured background intensity, $I_{s(p)\text{ref}}$ is the measured reflected intensity from the aluminum wafer, and $I_{s(p)\text{th,ref}}$ is the theoretical reflected intensity from a bare aluminum wafer.

III. EXPERIMENTAL DEMONSTRATION

In order to demonstrate our ability to accurately measure film thicknesses with the 2CSR we performed a series of experiments. In our first experiment, we studied the application of 2CSR to a silicon dioxide/silicon sample. We then applied the technique to a more complex structure, polysilicon/silicon dioxide/silicon. After establishing the quality of our static film thickness measurements, we performed etches of both the oxide and polysilicon films and monitored the film thickness *in situ* during these etches.

In this work we are etching nominally 1 μm silicon dioxide/silicon samples and stacks of roughly 5000 Å n^+polysilicon/300 Å silicon dioxide/Si. We model the n^+polysilicon as a bulk layer and a surface roughness layer to account for the roughness layer inherent to polysilicon.[15] We determined the index of refraction of these layers by performing *ex situ* SE measurements of the stack and fitting these data with the Bruggeman effective medium approximation.[39] These values were then fed into our optical model for the material.

Since we have both $|R_s|^2$ and $|R_p|^2$, we can fit either the 2CSR full data set, $|R_s|^2,|R_p|^2$, to an optical model or we can fit the ellipsometric parameter, $\tan(\psi)$, where $\tan(\psi) = (|R_p|^2/|R_s|^2)^{1/2}$ to an optical model. Looking at the data in the $\tan(\psi)$ mode, where the intensities are ratioed, affords us the same immunity that SE has to window coating and other situations where the overall intensity of the light varies during the course of a measurement. As a trade-off, though, when we fit in the $\tan(\psi)$ mode we are neglecting some of the information contained in the absolute intensity measurement of the 2CSR and, as is generally the case when taking the ratio of data, our noise increases. We will look at the effects of this later in this section.

Figure 5 shows the 2CSR measured reflectances, $|R_s|^2$ and $|R_p|^2$, and the best fits of these data from a nominally 10 000-Å-thick oxide on silicon. The best fit thickness of these data is 10 056 $\pm$ 2 Å, where the $\pm$2 Å is the statistical 95% confidence limit from the regression fit. This compares well with the result found by measuring the same film on an *ex situ* state-of-the-art scanning SE (10 076 Å). The quality of the fit shown in Fig. 5 indicates that when using the correct optical model for a material, 2CSR determines film thickness with an accuracy comparable to that of a slower, *ex situ* measurement tool.

Next, we looked at the more complex n^+polysilicon/silicon dioxide/silicon structure with the 2CSR. Figure 6 shows the 2CSR measured reflectances, $|R_s|^2$ and $|R_p|^2$, and the best fits of these data from the unetched polysilicon stack. In our optical model, we fixed the oxide thickness at 300 Å (as measured *ex situ* by SE) and fit both the roughness layer and bulk polysilicon thicknesses. The 2CSR measured bulk polysilicon and the surface roughness layer thicknesses are 5112 $\pm$ 3 and 48 $\pm$ 4 Å, respec-

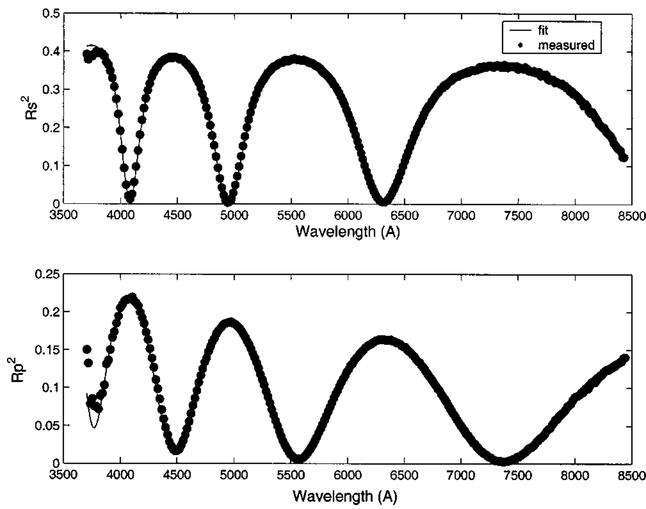

FIG. 5. 2CSR measurement (circles) and $|R_s|^2$ and $|R_p|^2$ fits (lines) of SiO_2 on Si; 45° polarization angle and 73° incident angle. Measured thickness is $10\,056\pm2$ Å where ±2 is the 95% confidence limit of the fit.

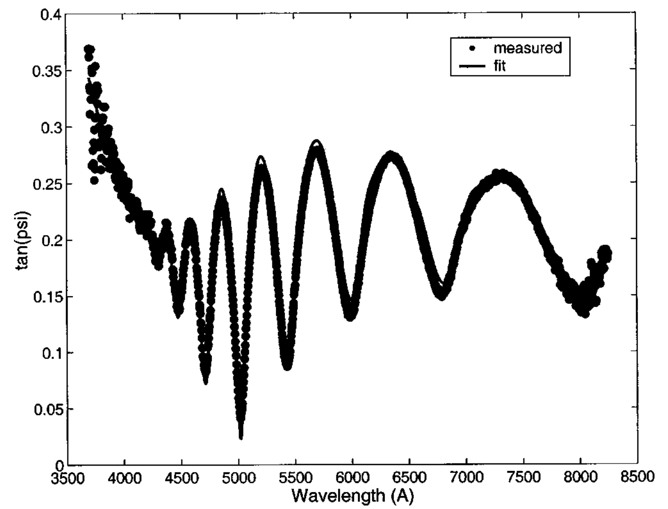

FIG. 7. 2CSR measurement (circles) and tan (ψ) fit of polysilicon/silicon dioxide/silicon SiO_2; 45° polarization angle and 73° incident angle. Bulk poly thickness is 5131 ± 1 Å with a 72 ± 2 Å surface roughness layer.

tively. *Ex situ* SE measurements of this sample show that the bulk polysilicon thickness is 5109 Å and the roughness layer thickness is 49 Å.

When we convert the $|R_s|^2,|R_p|^2$ data from the polysilicon measurement to the tan(ψ) mode, we obtain the fit shown in Fig. 7. The bulk polysilicon thickness is 5131 ± 1 Å and the surface roughness thickness is 72 ± 2 Å. As mentioned before, we lose some sensitivity to the film thickness when we ratio the *p*-reflected intensity to the *s*-reflected intensity, however, we gain the same immunity that SE has to intensity fluctuation issues such as window coating. We will further discuss the effects of fitting the tan(ψ) form of the polysilicon data when we look at measuring etch rates.

Despite the fact that our fit of the polysilicon data in the tan(ψ) mode returns roughly the same results as the $|R_s|^2,|R_p|^2$ fit, this is not the case for all materials. When we fit the same oxide data as that shown in Fig. 5 in the tan(ψ) mode, we get a thickness of 9988 ± 2 Å compared to the $|R_s|^2,|R_p|^2$ 2CSR measurement of $10\,056\pm2$ Å and the SE measurement of 10 076 Å. This discrepancy is due to the sharp discontinuities in the tan(ψ) data for this oxide (see Fig. 8). This problem of fitting points where tan(ψ) approaches infinity (low $|R_s|^2$) is encountered in SE measurements as well. In SE, it can be avoided by fitting the Fourier coefficients, α and β, rather than tan(ψ) and cos(Δ). In a rotating analyzer configuration α and β relate to the reflected intensity as in the following equation:

$$I_0(t)=I_0(1+\alpha\cos 2\omega_a t+\beta\sin 2\omega_a t), \tag{5}$$

where $I_0(t)$ is the time dependent reflected intensity and ω_a is the rotation frequency of the analyzer.[40] Thus, by fitting

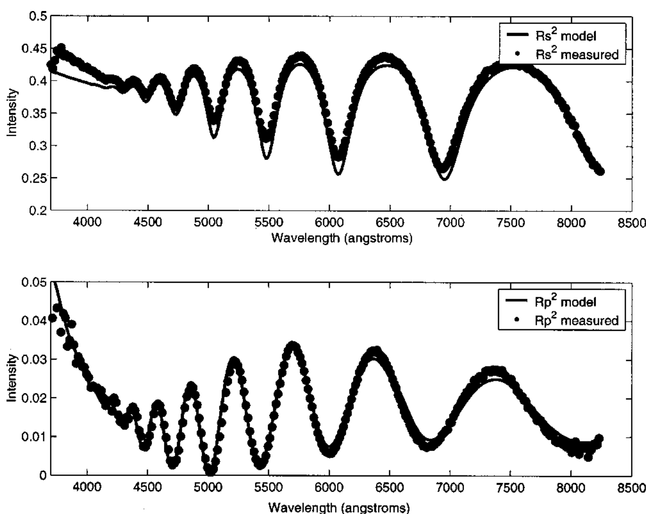

FIG. 6. 2CSR measurement (circles) and $|R_s|^2,|R_p|^2$ fits of blanket polysilicon on silicon dioxide sample; 45° polarization angle and 73° incident angle. The sample is modeled as 5112 ± 3 Å bulk polysilicon on 300 ÅSiO_2/Si with a 48 ± 4 Å surface roughness layer.

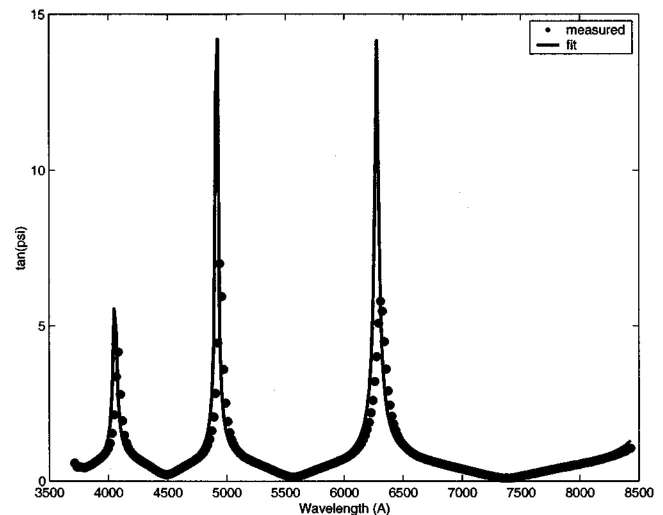

FIG. 8. 2CSR measurement (circles) and tan (ψ) fit of SiO_2 on Si; 45° polarization angle and 73° incident angle. Measured thickness is 9988 ±2 Å.

the raw data, α and β in rotating analyzer SE measurements and $|R_s|^2$ and $|R_p|^2$ in 2CSR measurements, rather than the ellipsometric parameters, the problems with fitting discontinuous data can, for the most part, be avoided.

We analyzed the noise in our thickness measurements by taking the standard deviation of repeated measurements of a sample with the plasma off. Similarly, we analyzed the noise in the etch rate by taking the standard deviation of a nominally constant etch rate. For all experiments we determined the etch rates by taking point-by-point derivatives of the thickness data. The standard deviation of our thickness for the SiO_2 samples, $\sigma_{d,\mathrm{ox}}$, is 0.22 Å where the thickness is determined from 30 averaged reflectance spectra, each spectra acquired in 6 ms. The standard deviation of our etch rate for the SiO_2 sample, $\sigma_{e,\mathrm{ox}}$, is 0.37 Å/s with the same integration time and sample averaging. This is in good agreement with our etch rate noise estimation for random noise sources shown in Eq. (6), which predicts $\sigma_e = 0.31$ Å/s:

$$\sigma_e = \sqrt{2}\sigma_d/\Delta t, \tag{6}$$

where Δt is the sampling time.[1] No pixel smoothing was done for the above measurements. If we perform three pixel boxcar smoothing, we find a standard deviation of 0.7 Å in repeated thickness measurements of a SiO_2 sample with a 6 ms integration time and no sample averaging. Without any pixel smoothing, the spectrometer has an optical resolution of 1.33 nm as stated earlier. By averaging over a total of seven pixels, we decrease the optical resolution to 2.22 nm, however, this does not adversely affect the quality of our data. More sophisticated smoothing algorithms, such as the Savitzky–Golay method,[41] can be used to improve the quality of these fits.

Likewise, we made repeated measurements of a n^+polysilicon/SiO_2/Si stack and determined the standard deviation of the measurements from both the $|R_s|^2,|R_p|^2$ and the tan(ψ) fits of the data. We find $\sigma_{d,\mathrm{poly}}$ to be 0.25 Å for the $|R_s|^2,|R_p|^2$ fit when we averaged over fifty 6 ms integration times for each thickness measurement. The standard deviation of the polysilicon etch rate, $\sigma_{e,\mathrm{poly}}$, is 0.32 Å/s from the $|R_s|^2,|R_p|^2$ fit where, again, the etch rate is determined by taking a point-by-point derivative of the thickness measurement. This is also in good agreement with our etch rate noise estimation from Eq. (6), from which we would expect $\sigma_{e,\mathrm{poly}}$ to be 0.35 Å/s.

When we find the noise in our thickness measurements for the tan(ψ) fit of the data, we find $\sigma_{d,\mathrm{poly}}$ to be 1.9 Å which is nearly eight times that of the $|R_s|^2,|R_p|^2$ fit. Similarly, the noise in the etch rate is 1.6 Å, five times higher than that found with the $|R_s|^2,|R_p|^2$ fit. These large standard deviations are due to the fact that, as stated earlier, taking the ratio of data amplifies any noise present in the original data.

In Fig. 9 we show 2CSR data from a CF_4 etch of a SiO_2 on Si sample. We fixed the pressure at 100 mTorr and the CF_4 flow rate at 50 sccm. The initial oxide thickness is 10 056 Å. We used a 6 ms integration time, averaged over 30 of these integration times and repeated this measurement once every second. We set the power at 50 W for the first

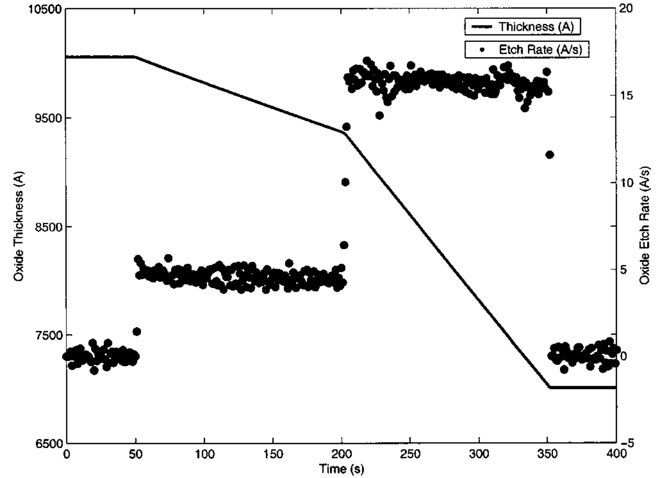

FIG. 9. SiO_2 etch in CF_4 at 100 mT with a power step from 50 to 100 W. The standard deviation of repeated thickness measurements is 0.22 Å and the standard deviation of the etch rate is 0.37 Å/s when fitting the data using $|R_s|^2$ and $|R_p|^2$.

150 s of the etch and increased it to 100 W for the second 150 s of the etch. The etch rate at 50 W is approximately 5 Å/s while the etch rate for 100 W is roughly 15 Å/s (see Fig. 9). The final oxide thickness is 7006 Å.

We show data from a CF_4 etch of the polysilicon/silicon dioxide/silicon stack in Fig. 10. Again, we fixed the pressure at 100 mtorr and the CF_4 flow rate at 50 sccm. We set the power at 50 W for the first 75 s of the etch and at 100 W for the second 75 s of the etch. The initial total polysilicon (bulk polysilicon+surface roughness layer) thickness is 5134 Å. The 50 W etch rate is approximately 7 Å/s and increases to roughly 20 Å/s when the power is increased to 100 W (see Fig. 10). The final total polysilicon thickness is 3140 Å. The oxide and polysilicon thickness measurements shown in Figs. 9 and 10 are determined by fitting the optical model for both $|R_s|^2$ and $|R_p|^2$.

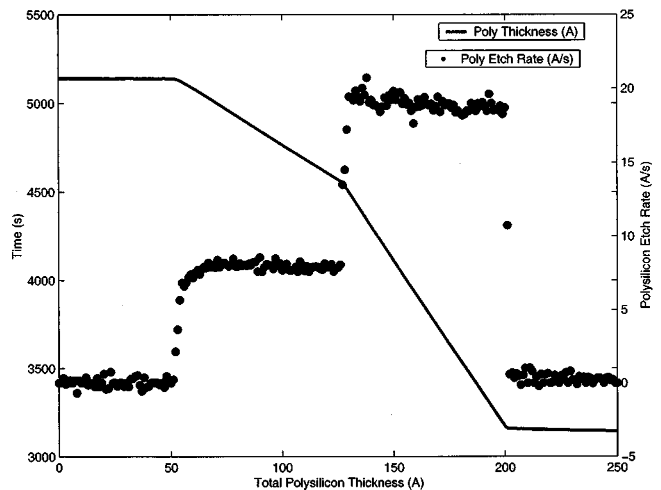

FIG. 10. Polysilicon etch in CF_4 at 100 mT with a power step from 50 to 100 W. The standard deviation of repeated thickness measurements is 0.25 Å and the standard deviation of the etch rate is 0.32 Å/s when fitting the data using $|R_s|^2$ and $|R_p|^2$.

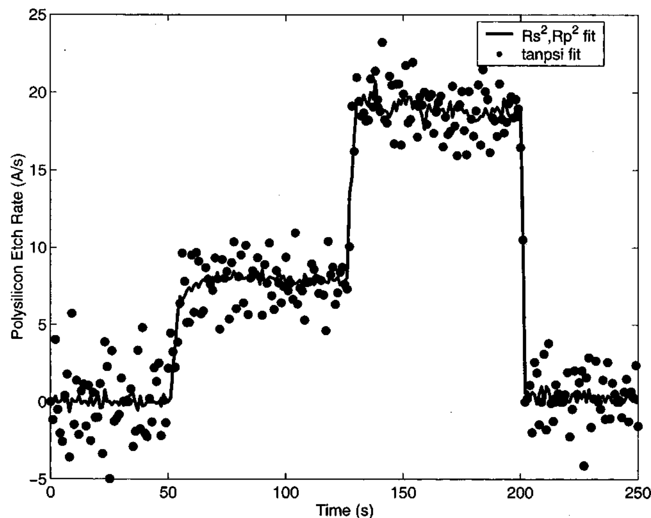

FIG. 11. Comparison of polysilicon etch rates from a $|R_s|^2$, $|R_p|^2$ fit and a tan (ψ) fit of the thickness. The standard deviation of the etch rate from the $|R_s|^2$, $|R_p|^2$ fit of the data is 0.32 Å/s while the standard deviation of the etch rate from the tan ψ fit of the data is 1.6 Å/s.

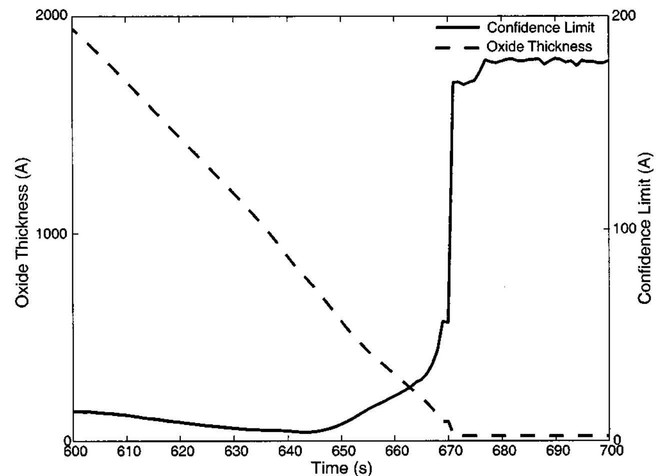

FIG. 12. Thickness and confidence limits as a function of time for the last 2000 Å of an oxide etch. When the oxide thickness decreases below roughly 600 Å, the 95% confidence limit on the best fit thickness value rises from roughly 10 Å to nearly 200 Å by the time the oxide thickness reaches 200 Å. Thus, for very thin oxides (those less than a few hundred angstroms) the 2CSR is not sensitive enough to provide accurate film thickness measurements.

In Fig. 11, we plot the same $|R_s|^2,|R_p|^2$ fit of the n^+polysilicon etch rate data shown in Fig. 10. We overlay these data with the equivalent etch rate data from the tan(ψ) fit (shown as circles in Fig. 11). The mean etch rate is the same for both fitting techniques, however, from Fig. 11 it is clear that the standard deviation of the data fit by the $|R_s|^2,|R_p|^2$ technique is substantially lower than that of the tan(ψ) fit as indicated in our standard deviation measurements.

Although 2CSR is better than SR at measuring very thin films, it is still important to note the limitations of the measurement. In Fig. 12, we show the thickness and the corresponding confidence limit on the thickness for a SiO_2 on Si sample as the final 2000 Å of material are removed during an etch. At the outset of this region of the etch, where the oxide thickness is nearly 2000 Å, the confidence limits are on the order of 10 Å. As the oxide thickness decreases below 600 Å (around 650 s), the confidence limits on the thickness begin to increase gradually until 665 s, when the confidence limits jump from 25 to 175 Å over the course of 10 s. This is the region where the oxide thickness is at and below 300 Å. Thus, as indicated by the large confidence limits on the film thickness fits below 300–400 Å, the 2CSR is not sensitive to very thin films. The phase information obtained in full SE measurements contains enough structure such that SE is able to more accurately quantify film thicknesses for well-characterized materials in the very thin film regime. The work of An *et al.* discusses combining SE and SR measurements which would better enable the measurement of these very thin films.[42]

Through these experiments on blanket wafers, we established that the 2CSR is able to accurately measure both blanket film thickness and etch rates. An evolving application of spectroscopic ellipsometry is the topographic analysis of grating structures. The diffraction from grating structures yields strong features in both tan(ψ) and cos(Δ). The linewidths, wall angles and more complex shape information of lines in gratings can be obtained from SE data by accurately modeling the diffraction from the grating.[43–46] Here, we will show that the 2CSR can perform similar measurements at high speeds. The first grating we have looked at is a 0.35 μm line/space grating in photoresist/300 Å SiO_2/Si (see Fig. 13). The period is measured as 0.700 μm using first order diffraction angle at multiple wavelengths. We measured the *s*- and *p*-reflected intensities from the grating using the 2CSR and we also measured the ellipsometric parameters at 73° incidence using a SOPRA GESP-5 *ex situ* SE. As with all of the other 2CSR measurements presented in this article, we used an integration time of 6 ms and, in this case, we did not perform any sample averaging.

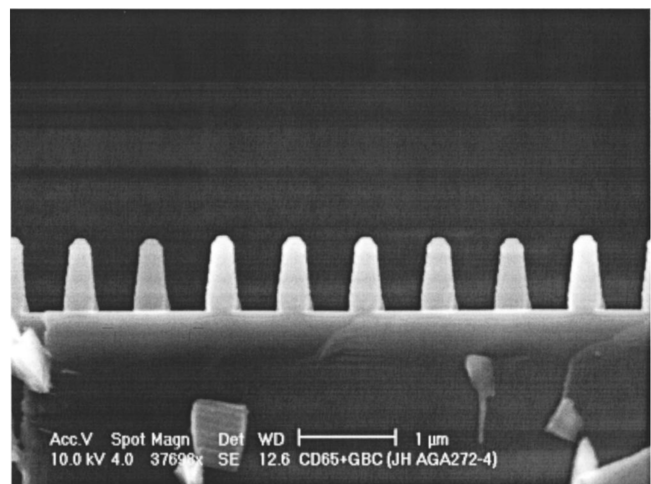

FIG. 13. SEM of 0.35 μm line/space photoresist grating on 300 ÅSiO_2 on Si. Photoresist thickness is approximately 0.8 μm.

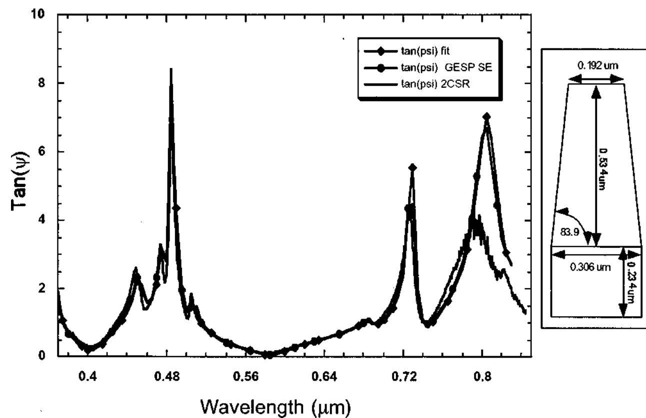

FIG. 14. $\tan\psi$ vs wavelength for a 0.35 μm line-space grating at 73° incidence. The degradation of the 2CSR signal at the higher wavelengths is due to the decreased sensitivity of the detector in this regime. Also shown is the geometrical model used in the RCWA analysis.

In addition to measuring $\tan(\psi)$ from complicated structures, we are also working on fitting the patterned structure data using the rigorous coupled wave analysis (RCWA) method.[47] We fix the oxide thickness at 300 Å. The grating is modeled as a trapezoid on a rectangular base (see Fig. 14) where we fit the top width, depth and wall angle of the trapezoid along with the depth of the rectangular base. The RCWA extracted best fit dimensions of the trapezoid are: top width$=0.192\,\mu$m, depth$=0.534\,\mu$m, and wall angle 83.9° and the depth of the rectangular base is 0.237 μm.

We plot the 2CSR measured data for $\tan(\psi)$ with the SE data and the RCWA fit in Fig. 14. Figure 14 clearly shows both the 2CSRs capability of accurately measuring $\tan(\psi)$ from complicated structures and our ability to fit the data with using the RCWA method. The 2CSR measurement, again, took on the order of milliseconds, while the *ex situ* scanning monochromator SE measurement took on the order of minutes to collect the same information. The noise in the 2CSR measurement in the infrared is due to the fact that the detector has its maximum efficiency between 2500 and 8000 Å.

IV. CONCLUSION

In this article we have presented a sensor for measuring thin films. This sensor, the 2CSR is a nondestructive, noninvasive thin film measurement tool with no moving parts which can be easily used for *in situ* metrology. The simplicity of the sensor, along with the recent availability of low-cost spectrometers with linear array detectors make the overall construction cost of the 2CSR low enough that this type of sensor can be implemented on a wide-scale basis in both research and industrial settings. The lack of moving parts and the linear array detectors afford us the ability to make high accuracy measurements on millisecond time scales. This high speed measurement capability makes the 2CSR ideal for process monitoring and industrial process control applications. With the fast data acquisition time, we can sample the *s*- and *p*-reflected intensities rapidly enough that we can detect transient phenomena not previously observable with the slower thin film measurement tools. With these data, we can develop a more complete understanding of the physics and chemistry of the etch process and apply this information to industrial process development and control issues. Additionally, we have shown that with 2CSR we have the level of accuracy needed to measure patterned wafer structure in a fraction of the time it takes conventional SE to make the same measurement. We also demonstrated our ability to fit these data using the RCWA method and to develop a model of the grating profile. When applied to etch measurements of patterned wafers, the RCWA method analysis of 2CSR data will allow us, in effect, to observe the grating profile evolution during an etch.

Our further development of the 2CSR may involve the transformation of the original sensor into an SE by adding a Fresnel Rhomb 1/4-wave achromatic compensator in either the polarizer-sample-compensator-analyzer mode or the polarizer-compensator-sample-analyzer mode. With the compensator set at 0°, we will obtain $|R_s|^2$ and $|R_p|^2$, as we do in our current polarizer-sample-analyzer two-channel spectroscopic reflectometry setup. With the compensator set to $\pm 45°$, we can obtain $|R_p+jR_s|^2$ and $|R_p-jR_s|^2$. So, with these measurements, we will be able to obtain ψ and Δ at high speeds with one three-position rotational moving part.

ACKNOWLEDGMENTS

This work was funded in part by the AFOSR/DARPA MURI Center for Intelligent Electronics Manufacturing under Contract No. AFOSR F49620-95-1-0524 and by the Semiconductor Research Corporation under Contract No. 97-FC085. The authors would like to thank C. Galarza, D. Grimard, D. Schweiger, P. Klimecky, M. Gulari, C. Garvin, A. Salian, and T. Li for their help in this work.

[1] T. Benson *et al.*, J. Vac. Sci. Technol. B **14**, 483 (1996).
[2] B. Rashap *et al.*, IEEE Trans. Semicond. Manuf. **8**, 286 (1995).
[3] K. McLaughlin, T. Edgard, and I. Trachtenberg, IEEE Control Syst. Mag. **11**, 3 (1991).
[4] N. Hershkowitz and H. Maynard, J. Vac. Sci. Technol. A **11**, 1172 (1993).
[5] S. Butler, K. McLaughlin, T. Edgar, and I. Trachtenberg, J. Electrochem. Soc. **138**, 2727 (1991).
[6] H. Maynard, N. Layadi, and J. Lee, Thin Solid Films **313–314**, 398 (1998).
[7] A. Heyd *et al.*, J. Vac. Sci. Technol. A **9**, 810 (1991).
[8] R. Collins, Rev. Sci. Instrum. **61**, 2029 (1990).
[9] N. Ianno *et al.*, Appl. Surf. Sci. **63**, 17 (1993).
[10] M. Li *et al.*, J. Vac. Sci. Technol. A **11**, 1686 (1993).
[11] N. Blayo, R. Cirelli, F. Klemens, and J. Lee, J. Opt. Soc. Am. A **12**, 591 (1995).
[12] P. Boher and J. Stehle, Mater. Sci. Eng., B **37**, 116 (1996).
[13] B. Hanyaloglu and E. Adyil, J. Vac. Sci. Technol. A **16**, 2794 (1998).
[14] K. Killeen and W. Brieland, J. Electron. Mater. **23**, 179 (1994).
[15] T. Benson, L. Kamlet, P. Klimecky, and F. L. Terry, Jr., J. Electron. Mater. **25**, 955 (1996).
[16] R. Azzam and N. Bashara, *Ellipsometry and Polarized Light* (Elsevier, New York, 1977).
[17] S. Henck, J. Vac. Sci. Technol. A **10**, 934 (1992).
[18] S. Henck, W. Duncan, L. Lowenstein, and S. Butler, J. Vac. Sci. Technol. A **11**, 1179 (1993).
[19] D. Aspnes, Proc. SPIE **946**, 112 (1988).
[20] G. Oehrlein, J. Vac. Sci. Technol. A **11**, 34 (1993).

[21]R. Collins, in *New Trends and Approaches in Electrochemical Technology*, edited by N. Masuko, T. Osaka, and Y. Fukunaka (VCH, New York, 1993), pp. 115–150.
[22]R. Collins, in *Semiconductor Interfaces Microstructures and Devices: Properties and Applications*, edited by Z. Feng (Institute of Physics, Philadelphia, PA, 1993), pp. 55–86.
[23]E. Irene, Thin Solid Films **233**, 96 (1993).
[24]N. Layadi, P. Roca i Caborrocas, B. Drevillon, and I. Solomon, Phys. Rev. B **52**, 5136 (1995).
[25]Y. Li *et al.*, Phys. Rev. Lett. **68**, 2814 (1992).
[26]I. An, Y. Li, H. Nguyen, and R. Collins, Rev. Sci. Instrum. **63**, 3842 (1992).
[27]N. Nguyen, B. Pudliner, I. An, and R. Collins, J. Opt. Soc. Am. A **8**, 919 (1991).
[28]I. An *et al.*, Thin Solid Films **206**, 300 (1991).
[29]K. Bachmann *et al.*, J. Cryst. Growth **183**, 323 (1998).
[30]N. Dietz, N. Sukidi, C. Harris, and K. Bachmann, J. Vac. Sci. Technol. A **15**, 807 (1997).
[31]B. Trotter, G. Moddel, R. Ostroff, and G. Bogart, Opt. Eng. **38**, 902 (1999).
[32]J. Archard, P. Clegg, and A. Taylor, Proc. Phys. Soc. London, Sect. B **65**, 758 (1952).
[33]R. Azzam, Opt. Acta **29**, 685 (1982).
[34]N. Smith, Phys. Rev. **183**, 634 (1969).
[35]G. Jellison and D. Lowndes, Appl. Opt. **24**, 2948 (1985).
[36]G. Jellison and F. Modine, Appl. Opt. **29**, 959 (1990).
[37]P. Hargis, Jr. *et al.*, Rev. Sci. Instrum. **65**, 140 (1994).
[38]D. Burge and H. Bennett, J. Opt. Soc. Am. **54**, 1428 (1964).
[39]D. Aspnes, J. Theeten, and F. Hottier, Phys. Rev. B **20**, 3292 (1979).
[40]D. Aspnes, in *Optical Properties of Solids: New Developments*, edited by B. Seraphin (American Elsevier, New York, 1976), pp. 799–846.
[41]A. Savitzky and M. Golay, Anal. Chem. **36**, 1627 (1964).
[42]I. An, H. Nguyen, A. Heyd, and R. Collins, Rev. Sci. Instrum. **65**, 3489 (1994).
[43]M. Lee *et al.*, *International Conference on Characterization and Metrology for ULSI Technology* (AIP, Woodbury, NY, 1998), Vol. 449, pp. 331–335.
[44]H. Huang *et al.*, *The 195th Meeting of the Electrochemical Society* (ECS, Pennington, NJ, 1999).
[45]H. Huang, W. Kong, B. Stutzman, and F. Terry, Jr., *AEC/APC Symposium* (SEMATECH, Austin, TX, 1999).
[46]N. Jakatdar, J. Bao, C. Spanos, and S. Yedur, Proc. SPIE **3677**, 159 (1999).
[47]M. Moharam and T. Gaylord, J. Opt. Soc. Am. **73**, 1385 (1982).